Research Article | Vol. 10, No. 9 / 1 September 2020 / Optical Materials Express 2274
Optical Materials EXPRESS

Impact of raw material surface oxide removal on dual band infrared optical properties of As_2Se_3 chalcogenide glass

Anupama Yadav,[1,2,*] Myungkoo Kang,[1] Claudia Goncalves,[1] Cesar Blanco,[1] Rashi Sharma,[1] and Kathleen Richardson[1]

[1]College of Optics and Photonics, CREOL, University of Central Florida, Orlando, FL 32816, USA
[2]Glass Division, CSIR-Central Glass and Ceramic Research Institute, Kolkata, WB 700032, India
[*]yadav.anupama@knights.ucf.edu

Abstract: The manufacturing of low loss chalcogenide glasses (ChGs) for optoelectronic applications is ultimately defined by the concentration of impurities present in starting materials or imparted via processing. We describe a rapid method for purifying metallic starting materials in As_2Se_3 glass where oxide reduction is correlated to optical and physical properties. Specifically, As-O reduction enhances the glass' dual-band optical transparency proportional to the extent (13-fold reduction) of oxide reduction, and is accompanied by a change in density and hardness associated with changes in matrix bonding. A significant modification of the glass' index and LWIR Abbe number is reported highlighting the significant impact purification has on material dispersion control required in optical designs.

1. Introduction

Chalcogenide glasses (ChGs) are being actively investigated due to their unique optical and physical properties, including the tailorability of optical function through compositional tuning. Chalcogenide glasses are promising for fabrication of optical fibers or in planar applications demanding low optical losses for chemical and biological sensing, as optical fibers in Raman lasers, amplifiers and for supercontinuum generation, in high speed switching, and other devices for systems spanning non-linear optics, photonics and telecommunications [1–7]. Despite their attractive attributes, the main challenge in producing low loss materials that require transmission over long path lengths, is synthesis of these glasses with ultra-high levels of chemical purity and physical compositional uniformity. Optical transparency in ChGs are driven intrinsically by glass forming network constituents and extrinsically by the level of impurities, most often affiliated with elemental starting materials and incomplete removal of moisture and/or surface oxide on starting material surfaces. The atoms of impurities, primarily O-, C-, and H- participating in the reactions of major components can redistribute between different molecular forms and functional groups and are responsible for the appearance of specific absorption bands in the transparency window of interest. The spectral position and intensity of absorption band can be used to determine the particular impurity and its relative content in the initial raw material and subsequent melt. The most frequently reported impurities with their extinction coefficient found in As_2Se_3 are summarized in Table 1. It is known that the optical transmission of ChGs and their use as optical media are impurity-sensitive, as impurities are the primary driver of loss which impacts the magnitude of launched light into a fiber or planar film which eventually arrives out. Such impurities in a ChG matrix not only increases loss, but can impact the glass' tendency towards crystallization and can result in selective impurity absorption bands and scattering [8–10]. Additionally, impurities have also been shown to directly impact post-draw fiber strength [11,12]. In view of increasing demand for higher performance chalcogenide optical fibers,

#400071 https://doi.org/10.1364/OME.400071
Journal © 2020 Received 12 Jun 2020; revised 8 Aug 2020; accepted 19 Aug 2020; published 26 Aug 2020

Optical Materials EXPRESS

fast, convenient and economical methods for the preparation of low loss ChGs are required. Furthermore, it is crucial to understand how the specific impurities impact the other optical properties of these glasses. Generally, low optical losses are expected for low content of limiting impurities, however, the influence of these impurities on mechanical properties and the refractive index dispersion are not well studied in the literature. To bridge the gap, goals of this research include the realization of low levels of absorption loss across the glass' full spectral window (i.e., for supercontinuum applications), targeted refractive index design (to enable splicing and other multi-material applications) and tailored dispersion behavior (for use in multi-material bulk, planar and fiber applications) [13–16].

Table 1. Impurity absorption bands and extinction coefficients reported for As_2Se_3 [8,17–20].

Impurity compound or functional group leading to absorption	Position of the maximum of the absorption band (μm)	Extinction Coefficient ($dBm^{-1}ppm^{-1}$)
OH^-	2.92	5.0
Se-H	4.55	1.0
As-H	5.02	-
H_2O	6.3	34
H_2Se/-Se-H	3.5	-
	4.1	-
	7.8	-
SeO_2	7.96	-
	8.7	-
Se-O	10.6	0.38
Si-O	9.2/9.5/10.0/10.4	-
Arsenic Oxides		
Glassy As_2O_3	7.5	0.09
	7.9	0.26
Glassy As_2O_3, claudetite	8.9	0.35
As_4O_6	9.5	1.03
As-O-H	10.8	-
As_4O_6	12.7	43.0
Glassy As_2O_3, claudetite	15.4	14.78

Chalcogenide glasses are most commonly produced by the co-fusion of elemental starting materials processed under vacuum in sealed quartz reaction tubes. The melt is rocked at melting temperature, T_m to ensure melt homogeneity and then is rapidly quenched in air or water, (or cooled using a defined cooling rate to ensure higher optical homogeneity), to freeze the material into an amorphous bulk structure. As-received, commercially available "high-purity" raw elements (such as those listed as 99.999% pure or 5N) are typically only analyzed for trace levels of metallic impurities. This purity rating does not reflect the presence of anionic/non-metallic impurities or adsorbed surface contamination. This is why commercial raw elements containing 0.01-0.1 ppm of metal impurities can routinely contain larger amounts (1-100 ppm) of hydrogen, oxygen and carbon impurities [21,22]. Embedded non-metallic impurities, stable dissolved compounds and heterogeneous inclusions make up the optically degrading constituents unaccounted for in vendor analysis, and such components can be largely attributable to the resulting glass' optical losses following melting. In addition to the starting elements, the potential for chemical interaction of chalcogenide and impurities with the silica glass ampoule used as the melting vessel at a high temperature can also be a source of hetero-phase inclusions in ChGs.

Optical Materials EXPRESS

Despite undergoing cleaning and 'bake out' protocols prior to being loaded with batch, these levels of ampoule surface contamination are typically small, as most ChG melting occurs at fusion temperatures below 1000°C. *Impurities transfer from the walls of silica glass ampoule into chalcogenide melt also depends on purity and fabrication technique of ampoules. The minimum content of hydrogen of 0.01 ppm wt in As_xS_{100-x} glass in the form of SH-groups was observed in the reactor from F300 tube with the content of OH-groups <1 ppm wt.* [23]. Any adsorbed impurities in or on the ampoule surface has a non-negligible diffusion coefficient that as in the case of hydrogen, can lead to the impurity entering the ChG melt during processing. Hydrogen content in quartz glass has been shown to be at levels of 100 ppm, and can enter the melt of ChG starting from 650 °C [24]. Hetero-phase inclusions can also lead to optical losses in ChG due to absorption and scattering and the extent of such impurity levels, while not often quantified, has been determined to be dominated by both concentration and particle size (0.05 – several μm) as calculated with scattering models of Mie and Rayleigh-Gans [25].

Great strides have been made in reducing optical losses in ChGs using improved purification techniques reported over the last decades. In these various methods, elemental starting materials are typically subjected to special purification measures like distillation, microwave assisted melting and synthesis over an $AlCl_3$ getter to achieve low levels of oxide impurities [26–31]. While shown to be effective, such purification protocols are not largely used in the routine manufacturing of ChGs as the techniques are both laborious and time consuming, often without yielding the desired ultra-high optical transparency in the spectral regime of interest. For the purpose of this research, conventional method of surface oxide removal from starting material is used for the preparation of low loss ChGs.

The aim of this work is to illustrate quantitatively, the role of surface oxide removal of the cationic elemental starting material (Arsenic, As) in the lab-scale production of bulk As_2Se_3 glass, and the impact of such processes on MWIR and LWIR optical properties of the resulting glass. Here, we specifically focus on the role of oxide content on the glass' transmission, refractive index and dispersion across these spectral windows. To perform the surface oxide removal process, heat treatment of elemental As starting material in chunks and powder form (to enhance the surface area) has been carried out using a facile method whereby material is treated under vacuum at temperatures where the vapor pressure of the oxide exceeds that of the parent As metal. For preferential volatilization of the oxide, heat treatment of As is performed in an open quartz ampoule connected to a dynamic vacuum system. For the current effort, only As starting material has been selected for surface oxide removal and no purification process has been performed on the parent glass' Se starting material. A comparison study of the As surface oxide removal on fabricated bulk As_2Se_3 material has been conducted by examining the change in transmission, refractive index dispersion, Raman spectra and Vickers hardness, associated with the pre- and post-removal of As surface oxide in the resulting binary compound. In our effort, we have assumed that any remaining residual oxide is dominated by that present in the untreated Se or from the melt environment, and as the source of this element remained constant throughout the study, it's quantity for the fixed size Se pellets in the constant size batch, was constant. The impact of the reduction in surface oxide originating on As starting material, is quantified in the physical property changes reported.

2. Experimental procedure

Vapor pressures of the commonly formed oxides of the elements of interest are several orders of magnitude higher than that for the corresponding 'pure' element. Thus, a way to purify or remove the surface oxide from elemental As chunks (nominally 3-6 mm in size) consists of heat treatment at 350 °C under vacuum to induce oxide volatilization. The duration of the purification process used in this study is 2 h. Furthermore, to enhance the surface area for surface oxide removal, As powder (pass through a sieve with nominal mesh aperture of 125 μm) is investigated

Optical Materials EXPRESS

to compare the effect of treatment on higher surface area material. Using the mean particle size of the treated chunks and powder (based on the assumption of a mean particle size and spherical particle shape) one can estimate that the specific surface area (surface-to-volume ratio) of As powder is 36 times more than As chunks. Thus for a common mass of as-batched As, the total surface area available for oxide removal treatment is much larger in finer sized, As powder. Here, post-sieved material is heated up to 350 °C for oxide removal, and held for the same 2 h period. In all processes of glass synthesis, strict temperature control is employed and the processes take place within a fume hood, ensuring a safe and continuous venting of all evolved species. The system was evacuated under vacuum (3.7×10^{-2} Torr). No cold trap and metallic getters have been used in this study.

Synthesis of 25 g of As_2Se_3 chalcogenide glasses is carried out by conventional melt-quenching technique. The appropriate amount of post-purified As-chunks or powder and Se starting materials are weighed and batched in a nitrogen purged, MBraun Labmaster 130 glove box. Purified As does not see ambient lab atmosphere as it is transferred via a fixed vacuum fixture to the glove box. The weighed batch is loaded into cleaned fused quartz tubes (10 mm in diameter) and seal under vacuum using a methane-oxygen torch to form sealed ampoules. All batches are melted in a rocking furnace overnight at a melting temperature of $T_m = 800$ °C. After overnight rocking at the melting temperature, the furnace temperature is reduced to the quench temperature, $T_Q = 600$ °C, prior to removal from the furnace for quenching using compressed air flowing over the ampoule. To minimize any quench-related stress, the prepared glasses are annealed at 140 °C for 2h and subsequently removed from the ampoule. The annealed glass rods are cut and polished to a final thickness of ~2 mm. Grinding is performed with SiC paper of fine grit sizes and the final polishing step is completed using 0.05 µm Al_2O_3 slurry. Table 2 summarizes the different purification protocols apply to both As chunks and powder in the present study, as compared to a melt where no purification was carried out.

Table 2. Purification protocols used in the study for As_2Se_3 ChG.

Sample Name	As- purification protocol
S_o	Unpurified
S_1	As-chunks purified at 350 °C for 2 h before batching
S_2	As-powder purified at 350 °C for 2h before batching

Sample S_o (referred to as unpurified) is obtained by the direct standard melting of high purity (5N) elemental starting materials (As and Se) without any heat treatment before batching. For Sample S_1, As-chunks (nominally 3-6 mm in size) are first purified. Heat treatment of As-chunks at 350 °C for 2 h is done under vacuum in order to remove surface oxide. After that purified As-chunks and as-available Se starting material are batched for the synthesis of As_2Se_3 glass. Similarly, for Sample S_2 As-powder pass through a sieve with nominal mesh aperture of 125 µm is heat treated at 350 °C for 2 hrs and later batched with Se to produce As_2Se_3 glasses. While the time period for the heat treatment has been selected on the basis of previous research work [26]. Heat treatment of As starting material has been carried out at temperature well below the sublimation temperature so that there is no weight loss during the heat treatment. Synthesis of all batches were carried out using the same procedure discussed earlier.

Fourier Transform Infrared (FTIR) Spectroscopy is performed on glasses to measure the transmission of polished samples. Two separate Perkin Elmer FTIR systems are used during the measurements. The Frontier FT-NIR model measures the transmission from 0.64-5 µm, while the Frontier Optica model measures transmission from 2-22 µm. The resolution of these systems is between +/– 1%.

Optical Materials EXPRESS

The structural properties of the glasses are investigated using a Bruker Senterra micro-Raman spectrometer. Raman scattering measurements are performed with an excitation laser wavelength of 785 nm with 1 mW power. Data is collected using a 30 second exposure and is accumulated over five scans. This has been checked by collecting the spectrum at the same spot thrice.

Pre- and post-processing measurements of the glass' physical properties include density and Vickers microhardness. Density is measured using the Archimedes principle with distilled water as immersion fluid at room temperature. Vickers microhardness, V_H, measurements have been performed on a Shimadzu DUH-211S Hardness Tester. Indentations are created on polished sample surfaces using a 100 mN load with a hold time of 10 seconds using a diamond indenter. The hardness tester is calibrated using a Ni metal calibration standard provided by Shimadzu. Sources of error can occur during this measurement if the sample does not have perfectly parallel surfaces (i.e., wedge) or if there is extensive pre-existing surface damage (cracks or scratches). The applied load has been chosen to be below the point where indentations created cracks emanating from the corners of the indent.

Refractive index is measured on samples using a Metricon Inc. prism coupler (2010M) that has been modified to measure the refractive index of bulk samples in the infrared region (from 1550 nm – 11 μm). Specific details on the system modification and basic principles of its use and measurements of index, dispersion and dn/dT on other chalcogenide glasses (in bulk and thin film form) can be found in works by Qiao et. al., Gleason et. al., Carlie et. al. [32–34]. In the present study, ten measurements are performed on each sample with an error of ± 0.0005. An undoped single crystal Ge prism (index range ~ 2.05 - 3.05 at 4.515 μm) is used for the measurements while a crystalline reference material (ZnSe) of known index is used as a calibration standard. Refractive index at different wavelengths across the MWIR and LWIR is measured at room temperature and fitted with a Sellmeier's equation.

3. Results and discussion

Optical transparency in ChGs is affected by the presence of undesirable impurities which leads to optical loss due to absorption and scattering in transmission spectra. Figure 1(a) shows the impact of purification protocol used in this study on the transmission spectra of As_2Se_3 bulk glasses. For comparison, the transmission spectra of a commercial sample (IRG 26) of nominally the same composition is also included in the figure. All samples under study exhibit transparency in the IR region; moreover, the multi-phonon edge at ~20 μm matches that for the As_2Se_3 composition previously reported in literature [28,35,36]. The identity of the species responsible for absorption loss and their spectral positions can be clearly associated with each functional group, and their respective magnitudes vary depending on the extent of purification of that sample. The band at 2.9 μm is associated with O-H groups, whereas the bands located near 6.3 μm are associated with the absorption lines of molecular H_2O. The bands at 3.5, 4.1 and 4.6 μm are associated with Se-H complexes, whereas the absorption bands in the region of 8.9 and 15.35 μm are attributed to absorption due to As-O impurities. Different forms of arsenic oxide impurities (As_4O_6, As_2O_3, As-O, As-O-As, As-O-H) can be seen to occur in the As_2Se_3 glass network with absorption features which span the 8-16 μm spectral range. These bands match with those previously reported in the literature [8,17–20,35].

The nature of the impurities in a glass material can essentially be determined by investigating the spectral dependence of the absorption coefficient, $\boldsymbol{\alpha}$ (cm^{-1}) and can be derived from Fresnel's formula. Thus for a bulk glass sample of thickness t, the absorption coefficient can be obtained from FTIR transmission data and using Beer-Lambert law [28,37,38]:

$$T = \frac{(1-R)^2}{(1-R^2)} e^{-\alpha t} \tag{1}$$

Optical Materials EXPRESS

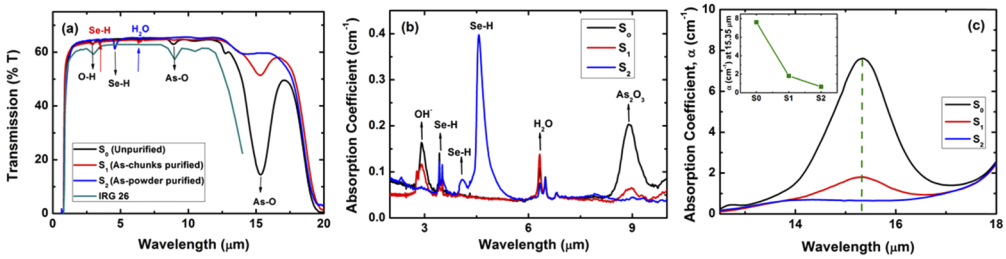

Fig. 1. (a) Infrared transmission spectra (corrected for thickness but not Fresnel loss) of purified and unpurified As_2Se_3 glasses. Data for the commercially available IRG 26 of the same composition (but different raw materials and processing protocol) is shown for comparison. The observed bands were assigned using earlier reported spectroscopic data on As_2Se_3 glasses. (b) Absorption coefficient, $\boldsymbol{\alpha}$ (cm^{-1}) of As_2Se_3 glasses in the spectral range of 2-10 μm synthesized using different purification protocols. Absorption coefficient has been determined from the transmission data using Eq. (1). (c) Enlarged view of the absorption coefficient, $\boldsymbol{\alpha}$ (cm^{-1}) in 12-18 μm spectral range to highlight the effect of purification protocol on the absorption band of As-O impurity at 15.35 μm. Inset shows the variation in $\boldsymbol{\alpha}$ (cm^{-1}) at 15.35 μm with purification. A 13-fold reduction in absorption coefficient can be seen with purification indicating that more oxide is present in the unpurified (Sample S_o) than those which have been purified (Sample S_1 and S_2).

where T is the transmittance from FTIR data, R is the reflection coefficient given by

$$R = \frac{(n-1)^2}{(n+1)^2} \tag{2}$$

and n is the glass' refractive index.

Using Eq. (1), the absorption coefficient, $\boldsymbol{\alpha}$ (cm^{-1}) of every glass sample is calculated over the entire spectral range and an attempt is made to quantitatively understand the change in glass' transparency due to impurities. Figure 1(b) shows the enlarged views of absorption coefficient in the 2-10 μm spectral range. The figure clearly shows the key features and impurity peaks in the MWIR spectral region. Despite the purification of the As starting material, the final As_2Se_3 glass samples still exhibit absorption impurities bands due hydrides (Se-H at 4.6 μm and O-H at 2.9 μm) and molecular water (6.3 μm) in the MWIR. However, one can notice that the amplitude of the bands related to oxygen (especially As-O at 8.8 μm) and water contamination is lower on purified melt as compared to unpurified except for Se-H impurities centered at 4.6 μm which shows an increase in concentration after the As powder purification. In the LWIR spectral region, the absorption band at 15.35 μm, the most intense in the measured glass' spectra have been expanded in Fig. 1(c) for emphasis. As seen in the Fig. 1(c), the main effect of the purification procedure in this study is observed in the As-O (15.35 μm) impurity band. This band, is ascribable to asymmetric As-O-As stretching vibrations in As_2O_3 structural units with As atom as constituent element and O atom incorporated as impurity in the As_2Se_3 network. For standard glass (S_o, referred to as unpurified), commercially available As-raw material (without any purification) is used and therefore intensity of As-O absorption coefficient is substantially higher, compared to the samples prepared after the purification (S_1 and S_2). Figure 1(c) inset shows the 13-fold reduction in absorption coefficient of 15.35 μm As-O band, indicating that more oxide is present the unpurified glass (Sample S_o) than those which have been purified (Sample S_1 and S_2). This is because for the unpurified glass, commercially available As starting material is sealed in the ampoule for batching and oxide impurities present in the element are trapped in the chalcogenide melt. But heat treatment of As elemental chunks under vacuum (Sample S_1) before batching separate the As element from its respective oxide while constantly evacuating oxide impurities.

Optical Materials EXPRESS

Additionally, surface oxide removal is more pronounced when purification is performed on the As powder (Sample S_2) as compared to the chunks. The much larger surface area exhibited by fine powder (pass through a sieve with nominal mesh aperture of 125 µm in size) as compared to chunks (3-6 mm in size) contributes to a significantly higher removal of the surface oxides and a more extensive decrease in the intensity of As-O absorption peaks is observed. This clearly shows that the reduction in absorption coefficient of As-O band is related to the surface oxides. Similar 7-fold reduction in As-O absorption coefficient (As_2O_3 structural unit) at 8.9 µm is also observed with purification and is shown in Fig. 1(b). Results from transmission spectra shows that purification protocol used in this study is extremely effective in reducing the intensity and concentration of the As-O constituents that dominate the MWIR and LWIR spectral region.

To quantify the evolution of the impurity content, concentration of impurity species has been extracted in glasses from their IR absorption coefficient spectra using the following relationship [26]:

$$[impurity] = \frac{\alpha_{dB/m}}{\varepsilon_{dB/(m.ppm)}} \tag{3}$$

where $\boldsymbol{\alpha}$ is the absorption coefficient (dB/m) and ε is the extinction coefficient (dB/m.ppm).

As shown in Table 3, purification protocol employed in this study drastically lowers the concentration of As-O impurities at 15.35 µm from 221 ppm to 17 ppm. In a similar manner, concentration of As-O impurity at 8.9 µm is shown to be reduced from 245 ppm to 37 ppm. The concentration of O-H and H_2O groups also shows a slight decrease with purification.

Table 3. Concentration of impurities as a function of purification protocol in As_2Se_3 glasses.

Impurity Bands	Extinction Coefficient, ε (dB/(m.ppm))	S_o		S_1		S_2	
		α (cm^{-1})	[impurity] ppm	α (cm^{-1})	[impurity] ppm	α (cm^{-1})	[impurity] ppm
OH^- *(2.9 µm)*	5.0	0.16	13.8	0.11	9.5	0.07	6.0
Se-H *(4.6 µm)*	1.0	0.04	17.2	0.04	17.2	0.37	159.1
H_2O *(6.3 µm)*	34.0	0.1	1.3	0.12	1.5	0.05	<1
As-O *(8.9 µm)*	0.35	0.20	245.7	0.06	73.7	0.03	36.9
(15.35 µm)	14.78	7.61	221.4	1.77	51.5	0.58	16.9

While the purification protocol applied in this study increase the surface oxide removal and causes the reduction in As-O band in the purified glass, one observes an increase in concentration of Se-H impurities centered at 4.6 µm after the As powder purification at 350 °C, seen in Fig. 1(b) and Table 3. Such a similar increase in the Se-H absorption band while producing ChG with distillation or getters has already been reported in the literature [26,39]. One proposed explanation suggests that as oxygen is removed from As starting material during purification, the resulting dissociation of the hydroxide to hydride result in hydride being recaptured by the Se during melting. As no efforts to capture hydride (such as through use of halide or other getters) have been made in this study, this is likely occurring in the glasses produced here. However, overall results from transmission spectra indicate that high temperature heat treatment of the As starting material before batching seems to be a feasible route to reduce surface oxides and thus improve the transmission spectra of the bulk glasses.

The molecular structure of As_2Se_3 glasses has been widely described as a random network of Se chain fragments crosslinked by $AsSe_{3/2}$ pyramidal units. The stoichiometric compositions of As_2Se_3 should theoretically have only As-Se hetero-polar bonds and the glass network should primarily consist of pyramidal structures made of 3-fold coordinated As and 2-fold coordinated Se. In reality, there is usually a small percentage of 'wrong'-bonding: homopolar bonds that

Optical Materials EXPRESS

form regardless of chemical order. Presence of oxygen as impurity in As_2Se_3 glass is believed to impact the glass' structure in two ways; firstly, it enters the glass network and decrease the glass network connectivity and, thus, increases the network's free volume. One might postulate that reduction in an oxygen containing network (as compared to one where oxygen has been present) would decrease the free volume and thus give rise to an increase in density. Additionally, since the As–O bond (484 kJ/mol) is notably stronger than the Se–O bond (419 kJ/mol) [40], oxygen is more likely to attach with As than Se. Secondly, replacing oxygen by Se affects the local polarizability and hence, can be correlated to changes in optical properties.

3.1. *Effect of surface oxide removal on the structural and mechanical properties of As_2Se_3 ChGs*

In order to investigate the effect of purification protocol on the structural properties of binary As_2Se_3 ChGs, Raman measurements were performed on the unpurified and purified samples. Figure 2(a) shows the Raman spectra of all three glasses. The strongest band centered at 225cm^{-1} in spectra of the glasses, is ascribed to $AsSe_{3/2}$ pyramidal units. As seen in figure purification protocols do not affect the Raman profiles and, consequently, the short-range order structure of glass matrix does not change. However, significant enhancement in the Raman band peak intensity at 225 cm^{-1} with purification of As-starting material could be related to the increase in the concentration of the $AsSe_{3/2}$ structural unit. As discussed earlier in Table 3 that surface oxide removal of elemental As starting material causes 13-fold and 7-fold reduction in As_2O_3 structural units at 15.4 and 8.9 μm. The relatively higher peak intensity of $AsSe_{3/2}$ band in the purified samples (Sample S_1 and S_2) suggests that some of the $AsO_{3/2}$ structures are replaced by $AsSe_{3/2}$. This can also be seen in Fig. 2(b) where Raman peak intensity at 225 cm^{-1} exhibits a trend that behave as $I(S_2) > I(S_1) > I(S_0)$ (I is peak intensity) whereas the concentration of As-O bonds exhibits exactly the opposite trend. The Raman intensity trend indicates that removing the surface oxide from As-raw materials before batching replace the As-O by As-Se in As_2Se_3 glasses.

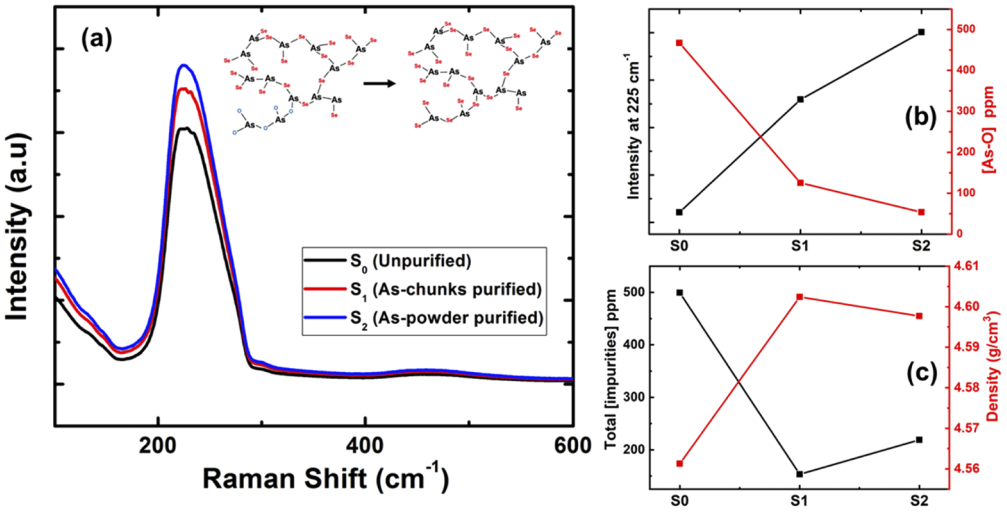

Fig. 2. (a) Raman spectra of unpurified and purified As_2Se_3 bulk glasses. (b) Change in Raman peak intensity at 225 cm^{-1} and concentration of As-O impurities as function of purification. (c) Concentration of total impurities (including OH^-, Se-H, H_2O and As-O) and density as a function of purification.

Optical Materials EXPRESS

Figure 2(c) shows that relation between the concentration of total impurities and density of glass with purification. Surface oxide removal causes a change in glass' network volume and mass by subsequent contraction of free volume. Additionally, the presence of oxygen containing species also has an impact on glass network connectivity. The reduction of As-O bonds after purification is responsible for the increase in the connectivity of glass network and the degree of compactness and, thus causes an increase in the density of As_2Se_3 glasses which further confirms the Raman intensity trend discussed above. On contrary, while surface oxide removal may lead to network strengthening, creation of Se–H dangling bonds after the powder purification at 350 °C decreases the glass' network connectivity and thus slightly reducing the density. The hydroxyl groups and molecular water are in very low concentration in these materials, but the generation of new Se–H bonds counterbalances and apparently outweighs the effect free volume contraction effect. The outcome of the surface oxide removal combined with Se-H increase results in overall increase in the density. Both Figs. 2(b) and (c) shows that experimental results of Raman spectra and density are in good accordance with the calculated impurities concentration. The results from Raman experiments are rather indirect observation of the effect of the raw material purification on the bulk glass but it does implicate the sensitivity of ChG towards the atmospheric contamination.

The hardness of a material corresponds to the resistance it opposes to the penetration of an indenter i.e., the glass' resistance to deformation. The indenter forces the inter-atomic lengths to expand or compress, but the inter-atomic forces and energies oppose the external force. As the force applied by indenter exceeds the average bond strength, the bonds will break apart and the material surface will start to deform plastically. Therefore, the materials with higher bong energy/strength exhibit higher hardness. In ChG, the structure of the glass and average bond strength forming the glass network determines the micro-hardness of the glass. Figure 3 shows the effect of purification protocol on Vickers micro-hardness of As_2Se_3 ChGs. In fact, the average bond strength of As-O (484 ± 8 kJ/mol) and O-H (429.91 ± 0.29 kJ/mol) bond is greater than As-Se (96 kJ/mole), As-As (385.8 kJ/mol), Se-Se (330.5 kJ/mole) and Se-H (312.5 kJ/mole) [40]. Purification of As-raw material causes the formation of As-Se bonds at the expense of As-O bond which is supported by FTIR and Raman data. In terms of mechanical properties, the increase in reticulation caused by the substitution of As-O bond by As-Se decreases the average bond strength in As_2Se_3 which further leads to the decrease in the micro-hardness of the glass from 1.511 ± 0.025 GPa (Sample S_o) to 1.473 ± 0.019 GPa (Sample S_1). This variation is above the level of error in the measurement. On the contrary, generation of new Se-H bonds slightly increases the average bond strength and results in increasing the microhardness of As_2Se_3 glass from 1.473 ± 0.019 GPa (Sample S_1) to 1.481 ± 0.02 GPa (Sample S_2). This variation is within the error of measurements, and thus one might can expect that the microhardness is more effected by large reduction in As-O impurities than increase in Se-H impurities.

3.2. Effect of surface oxide removal on the optical properties of As_2Se_3 ChGs

ChGs are of special interest for their high transparency towards the infrared but another attribute in usage of these glasses for infrared optical components is the refractive index and its dispersion behavior. Knowledge of the material's dispersion or wavelength dependence of refractive index is essential for the optical designers. Therefore, it is important to study the effect of the purification of starting raw elements (or reduction in surface oxide) on the refractive index dispersion of these glasses. The room temperature refractive indices of the glass samples were measured, and plotted in Fig. 4(a) as a function of wavelength and As purification protocol. First, one can observe a decrease of the refractive index with increasing the wavelength for each glass sample, showing thus their respective chromatic dispersion. Far from these resonances the real part of refractive index, $n(\lambda)$, can be approximated through the Sellmeier's equation:

$$n^2(\lambda) = A + \sum_i^I \frac{B_i \lambda^2}{\lambda^2 - C_i^2} \tag{4}$$

Optical Materials EXPRESS

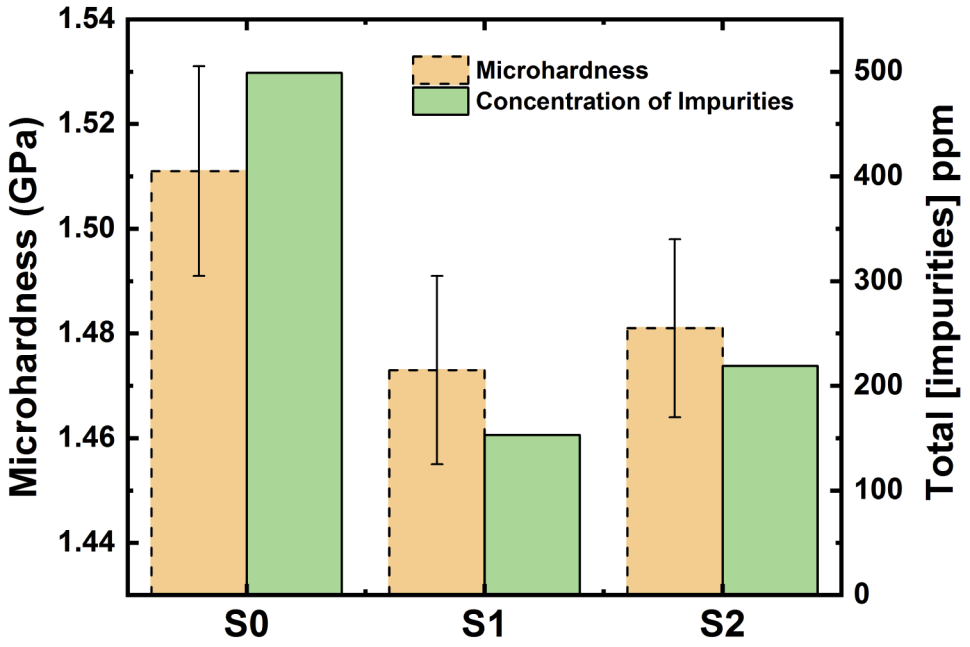

Fig. 3. Vickers micro-hardness of the bulk As_2Se_3 glasses as a function of purification protocol. Shown for comparison (right axis) is the calculated total impurity concentration. Figure illustrates the direct correlation of surface oxide removal on the mechanical property of the glass.

where A, B_i and C_i are Sellmeier's coefficients [41–43]. For the samples under study these coefficients are shown in Table 3. Even though Sellmeier equation is often expanded for $I > 2$ to phenomenologically account for refractive index values observed from the visible to the LWIR wavelengths. However, a three-term Sellmeier equation (including the constant term A, i.e., $I = 2$) is sufficient for fitting the continuous linear refractive index dispersion of bulk ChGs. The first and second term represent, respectively the contribution to refractive index due to higher-energy and lower-energy band gaps of electronic absorption, and the last term accounts for the decrease in refractive indexes due to lattice absorption. Here, the coefficient A is an approximation of the short-wavelength (e.g., ultraviolet) absorption contributions to the refractive index at longer wavelength. Considering this ChGs possess two absorption resonances in both ends of the optical transmission window, i.e., one located in the UV region and other in the IR region which correspond to C_1 and C_2, respectively. The second term of Eq. (4) incorporating C_1 affects the curvature of dispersion more significantly over the visible wavelengths, whereas the third term with C_2 does over the IR wavelengths [44].

Figure 4(a) shows the wavelength dependence of refractive index values for unpurified (Sample S_o) and purified glasses (Sample S_1 and S_2) as well as its fitted dispersion profile extracted from the Sellmeier equation. The refractive index values of commercial IRG 26 is also included for comparison. The slightly higher value of refractive index of commercial IRG 26 samples as compared to samples prepared in this study is likely due to the extremely different thermal histories and starting materials used to produce the glasses. Most 'academic' investigations involve small melt sizes with melting protocols far different from those used by commercial glass manufacturers preparing larger melt volumes and slower cooling rates required for realizing optical quality. The experimental evidence of variation in thermal history on corresponding impact on the resulting chalcogenide glass' optical and physical properties has already been

Optical Materials EXPRESS

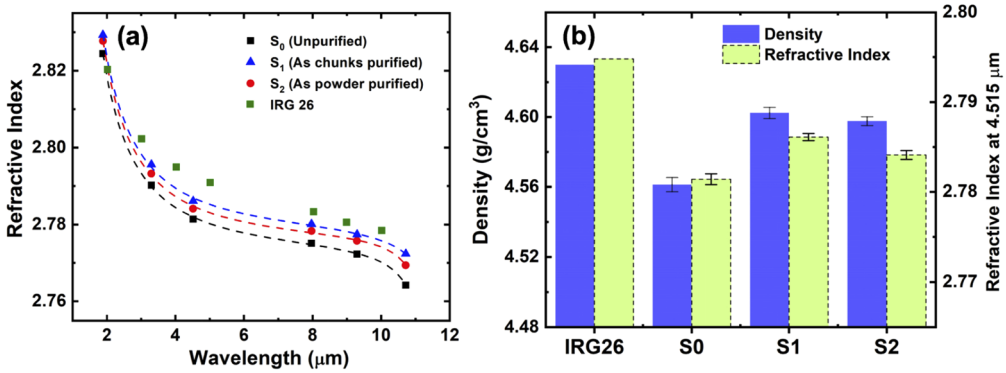

Fig. 4. (a) Measured linear refractive index (n) of unpurified and purified As_2Se_3 ChGs as a function of wavelength. The data have been fitted using the Sellmeier's dispersion formula (Eq. (4)). Values from this study and from commercial IRG 26 of same composition is included for comparison. Data for IRG 26 is taken from the product data sheet provided by the supplier (SCHOTT Glass). The difference in refractive index values for understudy and commercial IRG 26 samples is associated with markedly different thermal histories of glasses. (b) Variation of density and refractive index at 4.515 μm of unpurified and purified As_2Se_3 glasses with respect to the purification protocol. Refractive index value of IRG 26 is measured at 4 μm.

reported in the literature [45]. However, from Fig. 4(a), one can observe that the refractive index dispersion can be tailored via purification of As starting material. Replacement of As-O bond by As-Se bond into the glass network makes effective changes in the density and refractive index of the glass as shown in Fig. 4(b). Both density and refractive index of the purified glasses increases in comparison with reference unpurified glass. The change in density is related to the contraction of free volume and impact on glass network connectivity because of oxygen impurities. As discussed earlier, the outcome of the surface oxide removal leads to overall increase in the density of the sample S_1 and S_2 as compared to S_o, however combined with increase in the concentration of Se-H impurities in sample S_2 results in small decrease in the density as compared to S_1. A similar trend is observed in the refractive index of the bulk glasses as well. As one might expect that the change in the refractive index after purification is due to the (i) change in density caused by the structural rearrangement of As_2Se_3 glass network resulting from the termination of As-O bond (As_2O_3 structural units) (ii) change in mean polarizability caused by replacing oxygen by Se bonds. These data provide a much clearer representation of the significant refractive index fluctuations caused by the impurities in the glass melt.

The term chromatic dispersion emerges from the wavelength-dependence of the phase velocity of a light field when passing through an optical material or, in other words, from the variation of refractive index with wavelength. This phenomenon is usually quantified by the material's Abbe number, which accounts for a varying index of refraction with respect to specific, chosen wavelengths. The Abbe number is inversely proportional to the dispersion. Higher Abbe numbers indicate lower dispersion i.e the lower wavelength dependency of the refractive index. As seen in Table 4, there is a very small variation in Abbe number for SWIR $\left(\frac{n_2-1}{n_{1.6}-n_{2.4}}\right)$, and MWIR $\left(\frac{n_4-1}{n_3-n_5}\right)$ regions associated with purification protocol while As-raw material purification mostly affects the LWIR Abbe number $\left(\frac{n_9-1}{n_8-n_{10}}\right)$. It is evident that unpurified glass (Sample S_o) has drastically dispersion properties in LWIR spectral region, due to the stronger influence of infrared absorption bands on refractive index. The increase in LWIR Abbe number with purification is

Optical Materials EXPRESS

related to decrease in the absorption coefficient of As-O and is shown in Fig. 5(a). In general, purification of starting material leads to increase in the Abbe number. By varying the purification process, the refractive index of As_2Se_3 ChG can be tailor between 2.7814 (S_o) to 2.7861 (S_1) at 4.515 µm and the LWIR Abbe number can be tailor between 394 (S_o) to 480 (S_2).

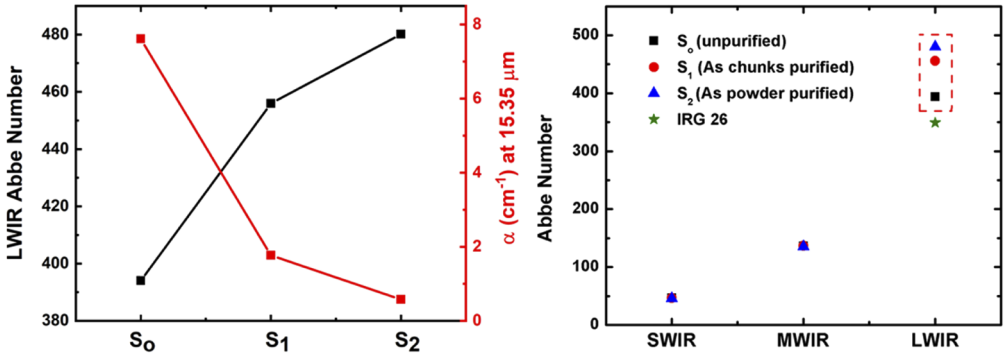

Fig. 5. (a) Variation in LWIR abbe number (v) absorption coefficient with purification protocol. (b) Compares the Abbe Number for SWIR (1.6 - 2.4 µm), MWIR (3 - 5 µm) and LWIR (8 - 10 µm) spectral region before and after purification. Purification of raw material have no significant effect on SWIR and MWIR Abbe Number while it mostly effects the LWIR Abbe Number.

Table 4. Optical constants including Sellmeier coefficients determined for unpurified and purified As_2Se_3 glasses based on the refractive index measurements using prism coupling technique. Abbe number for SWIR (1.6–2.4 µm), MWIR (3–5 µm) and LWIR (8–10 µm) spectral region. Optical constants of a commercial As_2Se_3 glass (Schott IRG 26) is included for reference.

Composition and Optical Constants		S_0 (unpurified)	S_1 (As chunks purified)	S_2 (As powder purified)	IRG26
Sellmeier Coefficients $n = \sqrt{A + \frac{B_1\lambda^2}{\lambda^2 - C_1^2} + \frac{B_2\lambda^2}{\lambda^2 - C_2^2}}$		A = -22.88211 B_1 = 30.57365 C_1 = 0.18105 B_2 = 0.0087 C_2 = 11.474	A = -23.49413 B_1 = 31.2139 C_1 = 0.17916 B_2 = 0.01122 C_2 = 12.05285	A = -22.822 B_1 = 30.52834 C_1 = 0.18238 B_2 = 0.00639 C_2 = 11.44227	A = 4.8535 B_1 = 3.0914 C_1 = 0.5352 B_2 = 1.0434 C_2 = 39.0459
SWIR	Linear Refractive Index	2.8439 at 1.6 µm 2.8185 at 2 µm 2.8047 at 2.4 µm	2.8488 at 1.6 µm 2.8235 at 2 µm 2.8097 at 2.4 µm	2.8475 at 1.6 µm 2.8217 at 2 µm 2.8077 at 2.4 µm	2.8199 at 2 µm
	Abbe Number	46.39	46.64	45.77	
MWIR	Linear Refractive Index	2.7933 at 3 µm 2.7844 at 4 µm 2.7802 at 5 µm	2.7983 at 3 µm 2.7895 at 4 µm 2.7852 at 5 µm	2.7963 at 3 µm 2.7873 at 4 µm 2.7831 at 5 µm	2.8017 at 3 µm 2.7948 at 4 µm 2.7910 at 5 µm
	Abbe Number	136.21	136.60	135.40	167.74
LWIR	Linear Refractive Index	2.7747 at 8 µm 2.7731 at 9 µm 2.7702 at 10 µm	2.7797 at 8 µm 2.7781 at 9 µm 2.7758 at 10 µm	2.7778 at 8 µm 2.7764 at 9 µm 2.7741 at 10 µm	2.7833 at 8 µm 2.7809 at 9 µm 2.7782 at 10 µm
	Abbe Number	394.02	455.92	480.11	349.19

Figure 5(b) and Table 4 compares the Abbe Number for SWIR, MWIR and LWIR spectral region. Purification protocol has slight effect on SWIR and MWIR Abbe Number. More

Optical Materials EXPRESS

importantly, the LWIR Abbe number is dramatically impacted (increased) when the oxygen present as an impurity species the glass' matrix reduced. Figure also compares the LWIR abbe Number with the commercially available As_2Se_3 glass (Schott IRG 26) for reference. Unpurified (sample S_o) glass' Abbe number being greater than those of commercial glasses does not necessarily mean that understudy glasses have a lower concentration of impurities as compared to that with in the commercial glasses. Abbe number is substantially influenced by many other factors (not just impurities) which in turn are dependent upon different thermal histories of glasses. However, for the glasses prepared by a well-characterized thermal history their Abbe number evolves as a function of the extent of its raw material's purification. Here, the larger Abbe number means less dispersion which in turn correlates with a lower absorption.

This study shows that both refractive index and dispersion are highly sensitive to the impurities. More importantly with purification of starting material, considerable dispersion shift can be obtained for the same composition. Precise tailoring of refractive index and dispersion can allow for a thermalization, reduction in number of components for color correction, and novel design forms. Thus, the ability to estimate the refractive index dispersion of glasses based on their absorption coefficient can provide an inroad for high-end optical designs and applications.

4. Conclusion

Although high purity raw elements are now commercially available, with 99.999% (5N) purity routine for many metals, even this level of purity is often not sufficient, particularly for optical fiber applications. For example, As_2Se_3 ChGs are good infrared transmitters and transmission window for these glasses can be extended to ~ 17 µm. However, presence of As-O absorption band at 15.35 µm shift the cutoff wavelength edge to 12.5 µm. To increase transparency towards the longer wavelength, it is necessary to eliminate this As-O absorption band through purification of elemental As starting material. In this study, bulk samples of As_2Se_3 chalcogenide glasses (ChGs) are synthesized by first removing surface oxide from elemental As before batching with Se. It is shown that as compared to As-chunks, powder of As material increases the surface area and consequently increases the surface oxide removal. Results from the experiments confirms that high temperature vacuum heat treatment of As-raw material powder before batching seems to be a feasible to reduce surface oxides and thus improve the transmission spectra of the bulk glass. Reduction in surface oxides impurities are correlated with the variation of glass' structural and mechanical properties. Impurity dependence of refractive index dispersion is also discussed with a special emphasis given to LWIR Abbe number in an effort to correlate the LWIR Abbe number with the As-O absorption coefficient. More specifically, the investigations of purified As_2Se_3 show that the refractive index dispersion can be tailored via purification of raw elements. These data have been compared to a commercially available material of similar composition. It has been shown that by appropriate engineering of the purification protocols, the dispersion can be tailored to the desired values, and by adopting new purification processes relatively low absorption losses are achievable. The results from this study will allow the optimization of the device design and processing steps necessary for those use in infrared photonics and sensing applications. Furthermore, As-O bond (484 kJ/mole) being stronger than Se-O bond (429 kJ/mole) suggest that oxygen has more tendency to form As-O bond than Se-O bond during melting of As_2Se_3 glass. This indicates that existence of As-O band at 15.35 µm is independent of whether oxygen is added to the glass melt from As or Se starting material. Therefore, we can assume that transmission could be enhanced even further by purification of Se starting material. Finally, increase in the degree of purity of starting materials for different glass forming system using present purification method can be considered as the direction for future research.

Optical Materials EXPRESS

Funding

University of Central Florida (Pre-eminent Post-doctoral Program (P3)); National Science Foundation (DMR-1506605); United States Department of Energy's National Nuclear Security Administration (DE-NA0002509).

Acknowledgments

The authors acknowledge the support of various funding sources, specifically, UCF's Pre-eminent Post-doctoral Program (P3) in their support of MK, CG and RS; AY, and KR were partially supported by NSF DMR-1506605 and DOE NNSA grant DE-NA0002509.

The authors would like to thank Dr. Clara Rivero-Baleine for helpful comments related to this topic area.

Disclosures

The authors declare no conflicts of interest.

References

1. V. S. Shiryaev and M. F. Churbanov, "Trends and prospects for development of chalcogenide fibers for mid-infrared transmission," J. Non-Cryst. Solids **377**, 225–230 (2013).
2. G. E. Snopatin, V. S. Shiryaev, V. G. Plotnichenko, E. M. Dianov, and M. F. Churbanov, "High-purity chalcogenide glasses for fiber optics," Inorg. Mater. **45**(13), 1439–1460 (2009).
3. J. Heo, M. Rodrigues, S. J. Saggese, and G. H. Sigel, "Remote fiber-optic chemical sensing using evanescent-wave interactions in chalcogenide glass fibers," Appl. Opt. **30**(27), 3944–3951 (1991).
4. M. Bernier, V. Fortin, N. Caron, M. El-Amraoui, Y. Messaddeq, and R. Vallée, "Mid-infrared chalcogenide glass Raman fiber laser," Opt. Lett. **38**(2), 127–129 (2013).
5. B. Bureau, C. Boussard, S. Cui, R. Chahal, M. L. Anne, V. Nazabal, O. Sire, O. Loréal, P. Lucas, V. Monbet, J. L. Doualan, P. Camy, H. Tariel, F. Charpentier, L. Quetel, J. L. Adam, and J. Lucas, "Chalcogenide optical fibers for mid-infrared sensing," Opt. Eng. **53**(2), 027101 (2014).
6. M. El-Amraoui, G. Gadret, J. C. Jules, J. Fatome, C. Fortier, F. Désévédavy, I. Skripatchev, Y. Messaddeq, J. Troles, L. Brilland, and W. Gao, "Microstructured chalcogenide optical fibers from As_2S_3 glass: Towards new IR broadband sources," Opt. Express **18**(25), 26655–26665 (2010).
7. J. S. Sanghera and I. D. Aggarwal, "Active and passive chalcogenide glass optical fibers for IR applications: a review," J. Non-Cryst. Solids **256-257**(256), 6–16 (1999).
8. M. F. Churbanov, G. E. Snopatin, V. S. Shiryaev, V. G. Plotnichenko, and E. M. Dianov, "Recent advances in preparation of high-purity glasses based on arsenic chalcogenides for fiber optics," J. Non-Cryst. Solids **357**(11-13), 2352–2357 (2011).
9. M. F. Churbanov, I. V. Skripachev, G. E. Snopatin, L. A. Ketkova, and V. G. Plotnichenko, "The problems of optical loss reduction in arsenic sulfide glass IR fibers," Opt. Mater. **102**, 109812 (2020).
10. A. Vaško, D. Ležal, and I. Srb, "Oxygen impurities and defects in chalcogenide glasses," J. Non-Cryst. Solids **4**, 311–321 (1970).
11. J. S. Sanghera and I. D. Aggarwal, "Development of chalcogenide glass fiber optics at NRL," J. Non-Cryst. Solids **213-214**, 63–67 (1997).
12. S. Danto, M. Dubernet, B. Giroire, J. D. Musgraves, P. Wachtel, T. Hawkins, J. Ballato, and K. Richardson, "Correlation between native As_2Se_3 preform purity and glass optical fiber mechanical strength," Mater. Res. Bull. **49**, 250–258 (2014).
13. I. Kubat and O. Bang, "Multimode supercontinuum generation in chalcogenide glass fibers," Opt. Express **24**(3), 2513–2526 (2016).
14. C. Goncalves, M. Kang, B. K. Sohn, G. Yin, J. Hu, D. T. H. Tan, and K. Richardson, "New candidate multicomponent chalcogenide glasses for supercontinuum generation," Appl. Sci. **8**(11), 2082 (2018).
15. M. Kang, L. Sisken, C. Lonergan, A. Buff, A. Yadav, C. Goncalves, C. Blanco, P. Wachtel, J. D. Musgraves, A. V. Pogrebnyakov, E. Baleine, C. Rivero-Baleine, T. S. Mayer, C. G. Pantano, and K. A. Richardson, "Monolithic chalcogenide optical nanocomposites enable infrared system innovation: gradient refractive index optics," Adv. Opt. Mater. **8**(10), 2000150 (2020).
16. J. L. Adam and X. Zhang, *Chalcogenide Glasses: Preparation, Properties and Applications* (Woodhead Publishing, 2014).
17. V. S. Shiryaev, S. V. Smetanin, D. K. Ovchinnikov, M. F. Churbanov, E. B. Kryukova, and V. G. Plotnichenko, "Effects of oxygen and carbon impurities on the optical transmission of As_2Se_3 glass," Inorg. Mater. **41**(3), 308–314 (2005).

Optical Materials EXPRESS

18. V. S. Shiryaev, M. F. Churbanov, E. M. Dianov, V. G. Plotnichenko, J. Adam, and J. Lucas, "Recent progress in preparation of chalcogenide As-Se-Te glasses with low impurity content," J. Optoelectron. Adv. M. **7**(4), 1773 (2005).
19. M. F. Churbanov, V. S. Shiryaev, S. V. Smetanin, V. G. Pimenov, E. A. Zaitseva, E. B. Kryukova, and V. G. Plotnichenko, "Effect of oxygen impurity on the optical transmission of $As_2Se_{3.4}$ glass," Inorg. Mater. **37**(11), 1188–1194 (2001).
20. W. A. King, A. G. Clare, and W. C. LaCourse, "Laboratory preparation of highly pure As_2Se_3 glass," J. Non-Cryst. Solids **181**(3), 231–237 (1995).
21. M. Churbanov, "Relevant problems of chemistry of high-purity substances," Inorg. Mater. **45**(9), 955–960 (2009).
22. L. Mochalov, A. Logunov, A. Kitnis, and V. Vorotyntsev, "Plasma-chemistry of arsenic selenide films: relationship between film properties and plasma power," Plasma Chem. Plasma Process. **40**(1), 407–421 (2020).
23. M. F. Churbanov, A. P. Velmuzhov, M. V. Sukhanov, G. E. Snopatin, I. V. Skripachev, and V. G. Plotnichenko, "Arsenic-sulfide glasses with low content of hydrogen impurity for fiber optics," Opt. Mater. **77**, 87–92 (2018).
24. M. F. Churbanov, "High-purity chalcogenide glasses as materials for fiber optics," J. Non-Cryst. Solids **184**, 25–29 (1995).
25. C. F. Bohren and D. R. Huffman, *Absorption and Scattering of Light by Small Particles* (John Wiley & Sons, 2008).
26. S. Danto, D. Thompson, P. Wachtel, J. D. Musgraves, and K. Richardson, "A comparative study of purification routes for As_2Se_3 chalcogenide glass," Int. J. Appl. Glass Sci. **4**(1), 31–41 (2013).
27. D. Thompson, S. Danto, J. D. Musgraves, P. Wachtel, B. Giroire, and K. Richardson, "Microwave assisted synthesis of high purity As_2Se_3 chalcogenide glasses," Phys. Chem. Glasses-Eur. J. Glass Sci. and Technol. Part B **54**(1), 27–34 (2013).
28. E. Guillevic, X. Zhang, J. L. Adam, H. Ma, J. Lucas, and H. Tariel, "Fabrication of highly homogeneous As_2Se_3 glass under argon flow," J. Non-Cryst. Solids **357**(15), 2897–2902 (2011).
29. T. Katsuyama, S. Satoh, and H. Matsumura, "Fabrication of high-purity chalcogenide glasses by chemical vapor deposition," J. Appl. Phys. **59**(5), 1446–1449 (1986).
30. K. Khan, *Manufacturing high purity chalcogenides* (Doctoral dissertation, University of Southampton, 2015).
31. J. S. Sanghera, V. Q. Nguyen, P. C. Pureza, F. H. Kung, R. Miklos, and I. D. Aggarwal, "Fabrication of low-loss IR-transmitting $Ge_{30}As_{10}Se_{30}Te_{30}$ glass fibers," J. Lightwave Technol. **12**(5), 737–741 (1994).
32. B. Gleason, K. Richardson, L. Sisken, and C. Smith, "Refractive index and thermo-optic coefficients of Ge-As-Se chalcogenide glasses," Int. J. Appl. Glass Sci. **7**(3), 374–383 (2016).
33. N. Carlie, N. C. Anheier Jr, and H. A. Qiao, "Measurement of the refractive index dispersion of As_2Se_3 bulk glass and thin films prior to and after laser irradiation and annealing using prism coupling in the near-and mid-infrared spectral range," Rev. Sci. Instrum. **82**(5), 053103 (2011).
34. H. A. Qiao, N. C. Anheier, J. D. Musgrave, K. Richardson, and D. W. Hewak, "Measurement of chalcogenide glass optical dispersion using a mid-infrared prism coupler," Proc. SPIE **8016**, 80160F (2011).
35. V. S. Shiryaev and M. F. Churbanov, "Recent advances in preparation of high-purity chalcogenide glasses for mid-IR photonics," J. Non-Cryst. Solids **475**, 1–9 (2017).
36. J. Lonergan, C. Smith, D. McClane, and K. Richardson, "Thermophysical properties and conduction mechanisms in As_xSe_{1-x} chalcogenide glasses ranging from x = 0.2 to 0.5," J. Appl. Phys. **120**(14), 145101 (2016).
37. C. T. Moynihan, P. B. Macedo, M. S. Maklad, R. K. Mohr, and R. E. Howard, "Intrinsic and impurity infrared absorption in As_2Se_3 glass," J. Non-Cryst. Solids **17**(3), 369–385 (1975).
38. T. F. Deutsch, ""Absorption coefficient of infrared laser window materials," J. Phys. Chem. Solids **34**(12), 2091–2104 (1973).
39. V. S. Shiryaev, J. L. Adam, X. H. Zhang, C. Boussard-Pledel, J. Lucas, and M. F. Churbanov, "Infrared fibers based on Te–As–Se glass system with low optical losses," J. Non-Cryst. Solids **336**(2), 113–119 (2004).
40. Y. R. Luo and J. A. Kerr, "Bond dissociation energies," in *CRC Handbook of Chemistry and Physics* (CRC Press, 2012).
41. J. H. Lee, J. H. Choi, J. H. Yi, W. H. Lee, E. S. Lee, and Y. G. Choi, "Unravelling interrelations between chemical composition and refractive index dispersion of infrared-transmitting chalcogenide glasses," Sci. Rep. **8**(1), 15482 (2018).
42. B. Tatian, "Fitting refractive-index data with the Sellmeier dispersion formula," Appl. Opt. **23**(24), 4477–4485 (1984).
43. G. Ghosh, "Sellmeier coefficients and dispersion of thermo-optic coefficients for some optical glasses," Appl. Opt. **36**(7), 1540–1546 (1997).
44. D. B. Tanner, *Optical Effects in Solids* (Cambridge University Press, 2019)
45. A. Yadav, A. Buff, M. Kang, L. Sisken, C. Smith, J. Lonergan, C. Blanco, M. Antia, M. Driggers, A. Kirk, C. Rivero-Baleine, T. Mayer, A. Swisher, A. Pogrebnyakov, A. R. Hilton, G. Whaley, T. J. Loretz, A. Yee, G. Schmidt, D. T. Moore, and K. A. Richardson, "Melt property variation in $GeSe_2$-As_2Se_3-PbSe glass ceramics for infrared gradient refractive index (GRIN) applications," Int. J. Appl. Glass Sci. **10**(1), 27–40 (2019).